JOURNAL OF THERMOPHYSICS AND HEAT TRANSFER
Vol. 19, No. 4, October–December 2005

Computation and Experiment of Nonequilibrium Nozzle Flow of Arc-heated Air

Ken-ichi Abe,* Tsuyoshi Kameyama,† and Hisashi Kihara‡
Kyushu University, Fukuoka 812-8581, Japan
Michio Nishida§
Sojo University, Kumamoto 860-0082, Japan
and
Katsuhiro Ito¶ and Hideyuki Tanno¶
Space Propulsion Research Center, Japan Aerospace Exploration Agency, Kakuta 981-1525, Japan

Numerical simulations of a nonequilibrium nozzle flow of arc-heated air were carried out using an eight-temperature model composed of translational, N_2-rotational, O_2-rotational, NO-rotational, N_2-vibrational, O_2-vibrational, NO-vibrational, and electron temperatures. The on-axis profile of each temperature in the nozzle is shown and the thermal characteristics of the nozzle flow are discussed. Measurements of NO emission spectra were also made at wavelengths 220–265 nm at the nozzle exit to determine NO rotational temperature by a curve-fitting method. Computed rotational temperature of NO at the nozzle exit was compared with the experimental temperature to discuss the nozzle flow model introduced to the present numerical analysis. Moreover, the present computation was applied to a nozzle flow in another arcjet facility. The comparison between the computed NO rotational temperature and the experimental temperature showed reasonable agreement.

Nomenclature

A	=	nozzle cross section
a	=	speed of sound
C_s	=	mass fraction of species s
E	=	total energy
e	=	internal energy
$\dot{e}_e$	=	production rate of electron energy due to inelastic collision
$\dot{e}_{\mathrm{rot},\,s}$	=	production rate of rotational energy of species s due to inelastic collision
$\dot{e}_{\mathrm{vib},\,s}$	=	production rate of vibrational energy of species s due to inelastic collision
h	=	enthalpy
h_s^0	=	formation energy of species s per mol
k	=	Boltzmann constant
M	=	Mach number
M_s	=	molecular weight of species s
$\dot{m}$	=	mass flow rate
N	=	number of species
P	=	arc power
p	=	pressure
Q_{T-R}	=	translation–rotation internal energy transfer rate per volume
Q_{T-V}	=	translation–vibration internal energy transfer rate per volume
Q_{T-e}	=	translation–electron internal energy transfer rate per volume
Q_{R-e}	=	rotation–electron internal energy transfer rate per volume
Q_{V-V}	=	vibration–vibration internal energy transfer rate per volume
Q_{V-e}	=	vibration–electron internal energy transfer rate per volume
q	=	heat flux
R	=	gas constant
T	=	temperature
t	=	time
u, v	=	velocity components in streamwise and radial directions, respectively
$V_{s,j}$	=	diffusion velocity of species s in the x_j-direction
x	=	axial coordinate
y	=	radial coordinate
η	=	efficiency of arc heating
Θ_{vib}	=	characteristic temperature for vibration
λ	=	thermal conductivity
ρ	=	density
τ	=	viscous stress

Subscripts

s	=	species s
e	=	electron
rot	=	rotation
tr	=	translation
vib	=	vibration
1	=	before arc heating
2	=	after arc heating

Received 22 September 2004; revision received 10 December 2004; accepted for publication 10 December 2004.

*Associate Professor, Department of Aeronautics and Astronautics; abe@aero.kyushu-u.ac.jp.
†Graduate Student, Department of Aeronautics and Astronautics.
‡Research Associate, Department of Aeronautics and Astronautics.
§Professor, Department of Aerospace Systems Engineering.
¶Senior Researcher. Member AIAA.

Introduction

AN arc-heated wind tunnel can well serve laboratory experiments on aerodynamic heating during atmospheric entry of space transportation systems and on surface catalysis of thermal protection material. However, it is extremely difficult to determine temperature, density, velocity, and species concentrations at the nozzle exit simultaneously. The numerical calculation of a thermochemical nonequilibrium nozzle flow from the discharge section to the nozzle exit is expected to be the most useful tool to determine such properties at the nozzle exit. Arc-heated high-temperature air is rotationally and vibrationally excited and partially dissociated and ionized. In the process of expansion of such high-temperature air in a nozzle,

energy transfers between internal energy modes take place. This process is in thermal nonequilibrium. Therefore, the nozzle flowfield analysis of high-temperature air needs thermal nonequilibrium treatment; namely, rotational and vibrational temperatures should be separated into those of each molecular species.

Babikian et al.[1] made spectroscopic measurements of NO band systems emitted from arc-heated air and determined NO rotational and vibrational temperatures at the nozzle exit. In addition, they compared these temperatures with those deduced from computations of a one-dimensional nonequilibrium nozzle flow and obtained a satisfactory agreement. Their computations used a five-temperature model of T_{tr}, T_{vib,N_2}, T_{vib,O_2}, $T_{vib,NO}$, and T_e and assumed that $T_{tr} = T_{rot}$. Babu and Subramaniam[2] conducted numerical simulations of a quasi-one-dimensional nozzle flow with a mixture of CO, Ar, and H_2 as test gas. Their thermal model was an equilibrium one. Park and Lee[3] made a validation of a multitemperature nozzle flow code by comparing numerically analyzed temperatures with two different sets of existing experimental data. They concluded that numerical calculations could approximately reproduce the existing experimental data taken in arcjet facilities. Thermochemical nonequilibrium in a supersonic freejet expansion of high-temperature air was numerically investigated by Nishida and Matsumoto[4] using multivibrational temperatures similar to those used by Babikian et al.[1] However, unlike Babikian et al.'s analysis, an axisymmetric flow model was adopted. A multi-vibrational-temperature model similar to that of Babikian et al.[1] was also introduced by Bourdon et al.[5] to their nozzle-flow simulations of N_2, O_2, NO, N, and O in high-temperature air. However, they still assumed that rotational temperature is equal to translational temperature. In their work, the influences of vibration–vibration and vibration–translation energy transfer rates on on-axis temperatures in the nozzle were investigated.

On the other hand, emission spectroscopy measurements in arcjet have been extensively carried out to determine rotational and vibrational temperatures. Winter and Auweter–Kurtz[6] measured emission spectra from N_2^+ and N_2 in an arc-heated air and determined their rotational and vibrational temperatures by a curve fitting method. Lago et al.[7] performed experimental simulations of an arc-heated Titan-like atmosphere (99% N_2 + 1% CH_4) and a Mars-like atmosphere (97% CO_2 + 3% N_2) and also determined the rotational and vibrational temperatures of CN, NH, and N_2^+ by means of a curve-fitting method.

Previous nozzle flowfield computations of high-temperature air assumed thermal equilibrium between translational and rotational temperatures. However, more accurate analysis needs to separately treat rotational temperature and furthermore to separate rotational temperature into those of molecular species, namely N_2 rotational, O_2 rotational, and NO rotational temperatures. In particular, in cases where rotational temperature deduced from optical emission spectroscopy is compared with that from numerical analysis of a high-temperature nozzle flow, the analysis of rotational temperature for each species is required. It is because of this that in the present study, thermal-nonequilibrium nozzle flow computation of high-temperature air was developed using an eight-temperature model consisting of translational, N_2-rotational, O_2-rotational, NO-rotational, N_2-vibrational, O_2-vibrational, NO-vibrational, and electron temperatures. Computed NO temperature at the nozzle exit is compared with the experimental one deduced from emission spectroscopy in an arcjet facility with air as the working gas. In addition, the present computation is applied to the nozzle flow at another arcjet facility and computed NO rotational temperature is compared with existing experimental data.

Nozzle Flow Computation

Analysis of Arc Heating

The arc heater considered in the computation is a conventional constrictor-type arc heater that has the same geometry as that used in the present experiment. The arc-heating of a test gas is modeled as described below. Although the test gas is actually arc-heated in the entire region of the constrictor, the discharge energy is injected into the test gas only at the end of the constrictor as shown in Fig. 1.

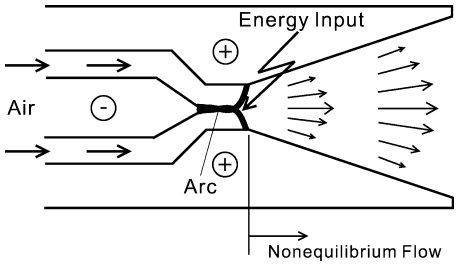

Fig. 1 Arc heater and nozzle.

Immediately after the heating, not only translation but also rotation and vibration are excited, and at the same time dissociations and ionizations take place. These processes instantaneously finish; namely, a thermochemical equilibrium state is instantaneously established at the end of the constrictor. Thus heated test gas is expanded through the divergent portion of the nozzle.

Equations of energy conservation and continuity for this heating process can be written respectively as

$$\dot{m}\left(h_1 + u_1^2/2\right) + \eta P = \dot{m}\left(h_2 + u_2^2/2\right) \tag{1}$$

$$\rho_2 u_2 A = \dot{m} \tag{2}$$

In Eq. (1), $\dot{m}(h_1 + u_1^2/2)$ is neglected, because it is sufficiently small compared with the input arc power. It is assumed that the arc-heated gas starts to expand into the divergent portion of the nozzle at a speed of sound, so we put $u_2 = a_2$. If $\dot{m}$, A, η and P are known, the state after heating can be determined from Eqs. (1) and (2) by using the computational code for thermochemical-equilibrium high-temperature air. The gas treated here is high-temperature air composed of N_2, O_2, NO, N, O, N_2^+, O_2^+, NO^+, N^+, O^+, and e^-. Species mass concentrations of original air are $C_{N_2} = 0.765$ and $C_{O_2} = 0.235$. First, equilibrium species mass fractions are determined by an approximate method; namely, they are calculated using a mean temperature that is constant in the radial direction. This temperature is obtained from the arc power in such a way as to satisfy $\dot{m}H = \eta P$, where H is the total enthalpy. This calculation is coupled with the calculation of equilibrium species mass fractions. Although a mean temperature is obtained, the temperature after heating, T_2, is expected to have a radial profile. Therefore in this study, as the first attempt, the radial profile of temperature is approximated by a connection of two parabolic curves. The wall temperature is kept at 1000 K and the on-axis temperature at the throat is determined so that the radial integral of enthalpy is equal to the injected arc power, that is, $\int \rho u H \mathrm{d}A = \eta P$, where the local velocity is assumed to be sonic and set equal to the local speed of sound calculated from local temperature and the local density was determined in such a way as to satisfy $\int \rho u \mathrm{d}A = \dot{m}$. Calculated properties are employed as upstream conditions for a nozzle flow analysis.

Model of a Thermal Nonequilibrium Nozzle Flow

The following assumptions are introduced into the nozzle flow analysis of high-temperature air:

1) The flow is axisymmetric and viscous.

2) A thermal nonequilibrium with eight temperatures is introduced: translational temperature (T_{tr}), rotational temperatures of individual molecular species (T_{rot,N_2}, T_{rot,O_2}, $T_{rot,NO}$), vibrational temperatures of individual molecular species (T_{vib,N_2}, T_{vib,O_2}, $T_{vib,NO}$), and electron temperature (T_e).

3) Chemical reactions in the nozzle are frozen.

A test calculation of nozzle flow taking into account chemical reactions returned a chemically frozen flow under the conditions used in the present analysis; thus all the present nozzle flow calculations were performed with a chemically frozen flow model.

Governing Equations

The steady-state nozzle flow is numerically calculated by integrating in time the unsteady equations and obtaining its large-time

limit. The problem is described by Navier–Stokes equations consisting of mass conservation, momentum, overall energy, molecular species s-rotational energy, molecular species s-vibrational energy, and electron energy equations in unsteady form. They are written as follows:

Mass conservation:

$$\frac{\partial \rho}{\partial t} + \frac{\partial (\rho u_j)}{\partial x_j} = 0 \tag{3}$$

Momentum:

$$\frac{\partial (\rho u_i)}{\partial t} + \frac{\partial (\rho u_i u_j)}{\partial x_j} = -\frac{\partial p}{\partial x_i} + \frac{\partial \tau_{ij}}{\partial x_j} \tag{4}$$

Overall energy:

$$\frac{\partial (\rho E)}{\partial t} + \frac{\partial [(\rho E + p) u_j]}{\partial x_j} = -\frac{\partial q_j}{\partial x_j} + \frac{\partial (u_i \tau_{ij})}{\partial x_j} \tag{5}$$

Rotational energy of molecular species s:

$$\frac{\partial (\rho_s e_{\text{rot},s})}{\partial t} + \frac{\partial (\rho e_{\text{rot},s} u_j)}{\partial x_j} = -\frac{\partial q_{\text{rot},s,j}}{\partial x_j} + Q_{T-R,s} + Q_{R-e,s} + \dot{e}_{\text{rot},s} \tag{6}$$

Vibrational energy of molecular species s:

$$\frac{\partial (\rho_s e_{\text{vib},s})}{\partial t} + \frac{\partial (\rho e_{\text{vib},s} u_j)}{\partial x_j} = -\frac{\partial q_{\text{vib},s,j}}{\partial x_j} + Q_{T-V,s} + Q_{V-V,s} + Q_{V-e,s} + \dot{e}_{\text{vib},s} \tag{7}$$

Electron energy:

$$\frac{\partial (\rho e_e)}{\partial t} + \frac{\partial (\rho e_e u_j)}{\partial x_j} = -\frac{\partial q_e, j}{\partial x_j} + p_e \frac{\partial u_j}{\partial x_j} + Q_{e-T} + Q_{e-R} + Q_{e-V} + \dot{e}_e \tag{8}$$

Total energy E is given by:

$$E = \sum_{s \neq e} C_s e_{\text{tr},s} + \sum_{s=M} C_s e_{\text{rot},s} + \sum_{s=M} C_s e_{\text{vib},s} + C_e e_e + \sum_{s=1}^{N} \frac{C_s}{M_s} h_s^0 + \frac{1}{2}(u^2 + v^2) \tag{9}$$

where $\sum_{s \neq e}$ denotes the summation over all species except electron and $\sum_{s=M}$ the summation over molecular species. Translational energy $e_{\text{tr},s}$, rotational energy $e_{\text{rot},s}$, and vibrational energy $e_{\text{vib},s}$ for species s are expressed as, respectively,

$$e_{\text{tr},s} = \left(\tfrac{3}{2}\right) R_s T_{\text{tr}} \tag{10}$$

$$e_{\text{rot},s} = R_s T_{\text{rot},s} \tag{11}$$

$$e_{\text{vib},s} = R_s \Theta_{\text{vib},s} / [\exp(\Theta_{\text{vib},s} / T_{\text{vib},s}) - 1] \tag{12}$$

$$e_e = \left(\tfrac{3}{2}\right) R_e T_e \tag{13}$$

where a rigid rotator model and a harmonic oscillator model are considered for molecular rotation and for molecular vibration, respectively. Overall, rotational, vibrational, and electron heat fluxes in the x_j direction are given by the following equations:

$$q_j = -\lambda_{\text{tr}} \frac{\partial T_{\text{tr}}}{\partial x_j} - \sum_{s=M} \lambda_{\text{rot},s} \frac{\partial T_{\text{rot},s}}{\partial x_j} - \sum_{s=M} \lambda_{\text{vib},s} \frac{\partial T_{\text{vib},s}}{\partial x_j} - \lambda_e \frac{\partial T_e}{\partial x_j} + \sum_{s=1}^{N} \rho_s h_s V_{s,j} \tag{14}$$

$$q_{\text{rot},s,j} = -\lambda_{\text{rot},s} \frac{\partial T_{\text{rot},s}}{\partial x_j} + \rho_s e_{\text{rot},s} V_{s,j} \tag{15}$$

$$q_{\text{vib},s,j} = -\lambda_{\text{vib},s} \frac{\partial T_{\text{vib},s}}{\partial x_j} + \rho_s e_{\text{vib},s} V_{s,j} \tag{16}$$

$$q_{e,j} = -\lambda_e \frac{\partial T_e}{\partial x_j} + \rho_e h_e V_{e,j} \tag{17}$$

The nozzle flow is assumed to be chemically frozen, so that $\dot{e}_{\text{rot},s} = 0$, $\dot{e}_{\text{vib},s} = 0$, and $\dot{e}_{\text{e}} = 0$.

Properties of High-Temperature Air

Transport Properties

The transport properties (viscosity, thermal conductivity, diffusion coefficient) can be calculated using the Yos formula,[8] which is based on the first Chapman–Enskog approximation. They were given by Gupta et al.[9]

Energy Transfer Between Internal Energy Modes

The energy transfers considered here are translation–rotation (T–R), translation–vibration (T–V), translation–electron (T–e), rotation–electron (R–e), vibration–vibration (V–V), and vibration–electron (V–e), as shown in Fig. 2.

T–R Energy Transfer

Lumpkin[10] and Parker[11] independently developed models for translation–rotation energy exchange rate. The Lumpkin model is based on experimental data of nitrogen and therefore it only applies to nitrogen. On the other hand, the Parker model can calculate the energy exchange rates for both nitrogen and oxygen. Hence, the Parker model was employed here. Parker gave the collision numbers only for nitrogen and oxygen. Because there are no available experimental data for NO, the collision number for NO is set to the average of those for nitrogen and oxygen in the present study.

T–V Energy Transfer

Vibrational relaxation in an expanding flow is faster than that behind a shock wave, so that Millikan and White's expression for vibrational relaxation time[12] must be divided by a factor of ϕ. The value of ϕ was proposed to be as follows[3]:

$$\phi_{\text{N}_2} = 1.5, \qquad \phi_{\text{O}_2} = 1.5, \qquad \phi_{\text{NO}} = 3$$

T–e Energy Transfer

The rate of translational energy transfer between heavy particles and electrons given by Lee[13] is used. The approximate expression for the collision cross section of electron–neutral particle encounters proposed by Gnoffo et al.[14] is used here. Coulomb cross section is employed for electron–ion encounters.

R–e Energy Transfer

The energy transfer between rotational and electron energy modes was also considered in the energy conservation equations. The expression for R–e energy transfer was obtained by extending the expression given in the work of Nishida and Matsumoto[4] to a multirotational-temperature model.

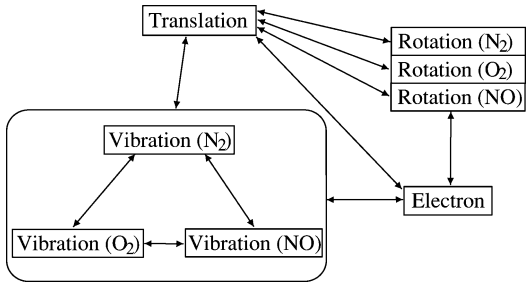

Fig. 2 Energy transfer between internal energy modes.

V–V Energy Transfer

The vibration–vibration energy transfer rate between two different molecular species used here is based on the work of Candler and MacCormack.[15] The energy transfer probabilities were taken from the work of Park and Lee.[3]

V–e Energy Transfer

The relaxation time for the nitrogen vibration–electron energy transfer rate was given by Lee.[16] The vibration–electron energy transfer cross sections for O_2 and NO are much smaller than that for N_2, so that the vibration–electron energy transfer relaxation times for O_2 and NO are used here by multiplying that for N_2 by 300 (Ref. 3).

Computational Results

Nozzle Entrance Conditions

Computations were made for the conditions of an arc-heated wind tunnel at the Department of Aeronautics and Astronautics, Kyushu University (KU), operated at a maximum arc power of 20 kW (Ref. 17). First, the nozzle entrance conditions, that is, the conditions immediately after arc heating, were determined with the present experimental conditions of arc power 12.8 kW, mass flow rate 0.43 g/s, and constrictor (nozzle throat) diameter 5 mm. Note that the heating efficiency was taken to be 0.4 according to Kim et al.[18] and Park et al.[19] Numerical results show $p = 36.2$ kPa, $T = 11{,}700$ K, and $u = 2.28 \times 10^3$ m/s on the axis. Although the computed equilibrium temperature is as high as 11,700 K, this temperature is merely the on-axis temperature and the temperature at the wall is kept at 1,000 K, as mentioned earlier. Computed species mass fractions are shown in Table 1. It is apparent that the dominant species are N_2, O, N_2^+, NO, O_2, and NO^+. Radial profiles of temperature and total enthalpy are shown in Fig. 3, and those of velocity and density in Fig. 4.

Nozzle Flow Field

A set of governing equations are numerically solved using the second-order upwind total variation diminishing scheme of Harten–Yee type[20] for the convection terms and the second-order central difference for viscous, heat-conductive, and diffusive terms. Calculations used the same nozzle geometry as in the present experiments, which is such that the divergent portion is conical in shape, nozzle throat (entrance) diameter is 5 mm, nozzle exit diameter is 100 mm,

Table 1 Species mass fractions at throat

N_2	O	N_2^+	NO	O_2
7.03×10^{-1}	1.38×10^{-1}	6.14×10^{-2}	3.78×10^{-2}	3.69×10^{-2}
NO^+	N	N^+	O_2^+	O^+
2.24×10^{-2}	3.60×10^{-4}	2.93×10^{-8}	3.40×10^{-12}	5.52×10^{-14}

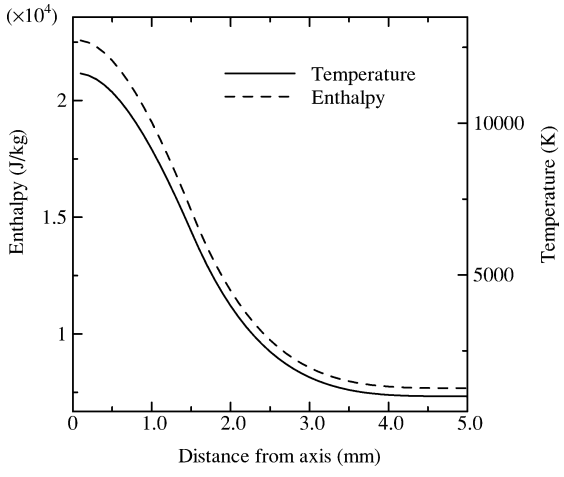

Fig. 3 Radial profiles of temperature and enthalpy at throat.

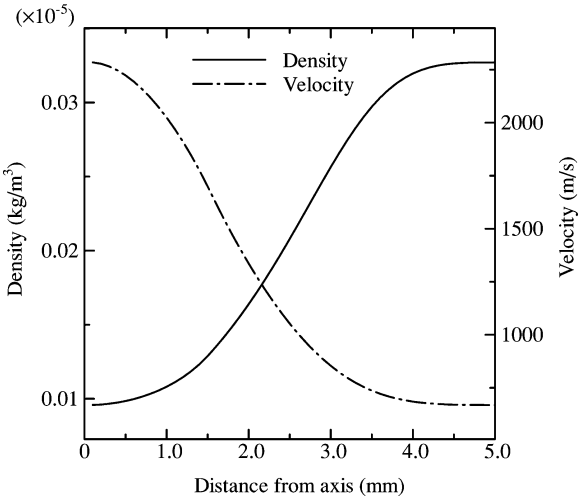

Fig. 4 Radial profiles of velocity and density at throat.

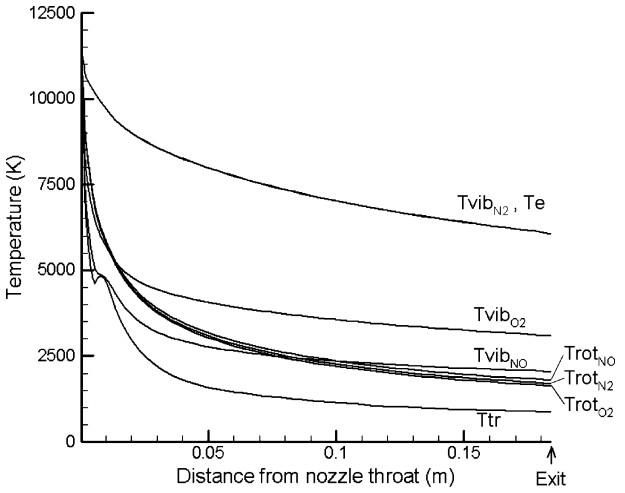

Fig. 5 On-axis temperature profiles.

and nozzle cone half angle is 15 deg. The nozzle entrance conditions determined in the preceding section serve as the upstream boundary conditions. No slip conditions are imposed on the nozzle wall; that is, $u = v = 0$ and equitemperature of 1,000 K was assumed at the nozzle wall.

On-axis temperatures obtained from the axisymmetric nozzle flow computation are shown in Fig. 5. There is a small kink in the vicinity of the nozzle throat. This is due to a weak oblique shock generated inside the nozzle. It can be seen that T_{vib,N_2} and T_e are completely in equilibrium. This strong coupling is owing to the fact that the energy transfer rate between the vibrational energy mode of nitrogen and electron energy mode is much higher than those between other molecular species and electrons.[3] Rotational temperatures of N_2, O_2, and NO are nearly in equilibrium with each other. However, they are completely in nonequilibrium with translational temperature. This evidence shows a need at least to separate rotational temperature from translational temperature. It can be also seen that O_2 vibrational temperature is less than rotational temperature in the vicinity of the throat and that NO vibrational temperature is less than rotational temperature in the upstream half region of the nozzle. Park has already shown similar features.[21] He explained that the relaxation of vibrational temperature to translational temperature is faster than that of rotational temperature in high-temperature regions. According to the present calculations, the R–e energy transfer was negligibly small compared with the T–R energy transfer under the present conditions.

Computed flow properties on the centerline at the nozzle exit are pressure 11.9 Pa and Mach number 6.54. On-axis temperatures at the nozzle exit are shown in Table 2. This table shows

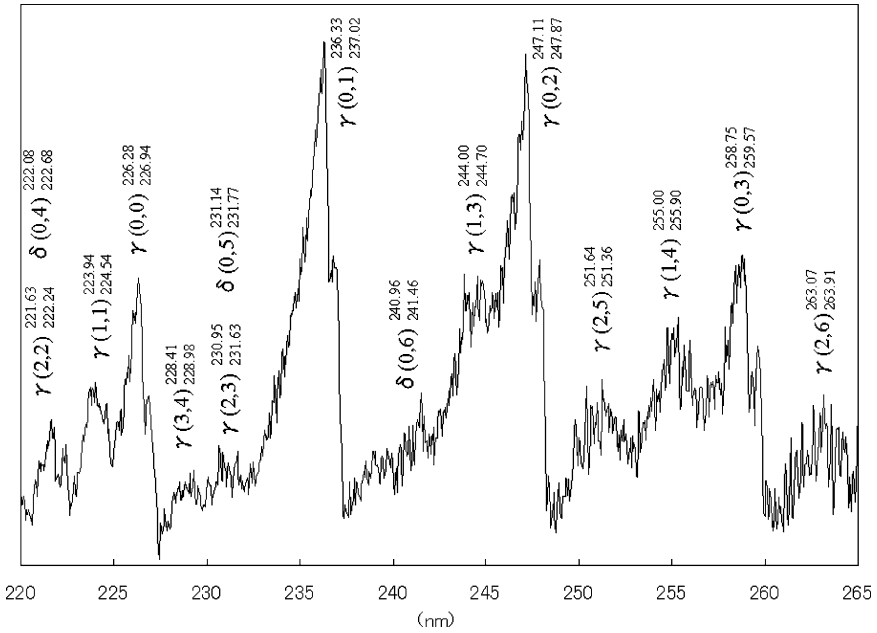

Fig. 6 Emission spectra from arc-heated air.

Table 2 Computed temperatures at nozzle exit (K)

T_{tr}	T_{rot,N_2}	T_{rot,O_2}	$T_{rot,NO}$
850	1,700	1,600	1,800
T_{vib,N_2}	T_{vib,O_2}	$T_{vib,NO}$	T_e
6,100	3,100	2,000	6,100

$T_{vib,N_2} > T_{vib,O_2} > T_{vib,NO} > T_{tr}$. This feature coincides with the conclusion of Park and Lee.[3] At the nozzle exit, $T_{vib,NO}$ is slightly larger than all the rotational temperatures. This is due to the nozzle entrance conditions (conditions after arc heating) and nozzle geometry. NO rotational temperature at the nozzle exit will be compared with the experimental one later.

Spectroscopic Measurements

Emission spectra of NO of arc-heated air at wavelengths of 220–265 nm were measured in an arc-heated wind tunnel in KU. As mentioned earlier, the arc heater is connected to a nozzle of 5 mm in entrance diameter, 100 mm in exit diameter, and 15 deg in cone half angle. Arc-heated air is expanded through the nozzle and is discharged into a cylindrical test chamber 1 m in length and 1 m in diameter. It is repeated that experimental conditions were such that the mass flow rate of the test gas was 0.43 g/s and arc power was 12.8 kW. The corresponding enthalpy was 29.8 MJ/kg.

Only the radiation emitted from the center axis at the nozzle exit was focused onto a multichannel spectrometer. Spectral intensities were then detected by an image-intensified charge-coupled device (ICCD) camera. The spectrometer has an entrance slit of 10 μm width, 25 cm focal length, and a flat plate grating of 1800 lines/mm. The detector of the spectrometer is an ICCD camera with 576×384 pixels, mounted on the spectrometer. The spectral resolution of the analysis system is 0.04 nm per pixel. The CCD was cooled to 243 K to reduce thermal noises. The exposure time was taken equal to 1 s. The spectral responses of the present grating and ICCD are flat over the wavelength range of interest, 220–265 nm.

Measured spectra at wavelengths 220–265 nm are shown in Fig. 6. NO band spectra, which are typical in high-temperature dissociated air, can be observed. The NO $\gamma(0,1)$ band spectra are not disturbed by other NO spectra, so they were selected to determine rotational temperature of NO by a curve-fitting procedure.

Figure 7 illustrates the curve fitting using SPRADIAN, which is a computational code for spectral intensity and radiative heat flux

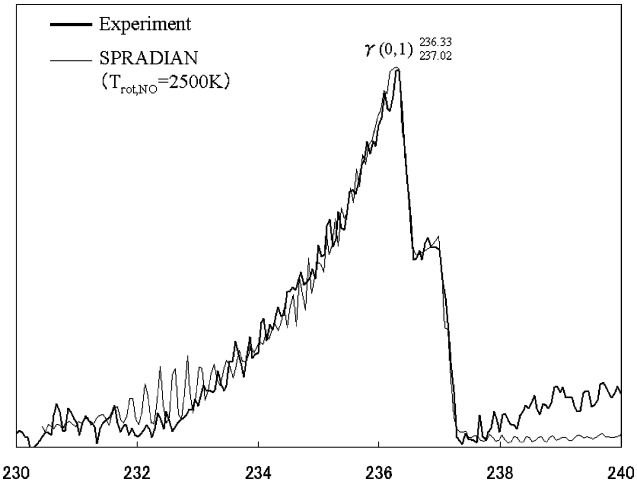

Fig. 7 Curve fitting using SPRADIAN (Fujita and Abe[22]).

developed by Fujita and Abe.[22] The determined NO rotational temperature is 2500 ± 50 K. This error is caused by that in the curve fitting. The experimental temperature is compared with the computational temperature of 1800 K. This comparison shows that the computed NO rotational temperature is 28% lower than the measured one. Although the current model performance is not perfect, it may be mentioned that the present computation can predict NO rotational temperature within an error of about 30% for this arc-jet facility. Further discussion on the model performance will be given later by comparison to the results for another facility.

Comparison with Other Experiments

Watanabe et al.[23] measured NO spectra in a 750-kW arc-heated facility at the National Aerospace Laboratory (NAL), Japan. This facility has a segment-type arc heater connected to a nozzle 25 mm in entrance diameter, 115 mm in exit diameter, and 15 deg in cone half angle. Using a curve-fitting method, they determined NO rotational temperatures from band spectra of $\delta(0,1)$, $\delta(0,2)$, $\delta(0,3)$, $\gamma(0,0)$, and $\gamma(0,1)$. Their results are shown in Table 3. The present nozzle computation was applied to the nozzle flow of arc-heated air at the NAL facility, and the computed NO rotational temperature was compared with the experimental one. Experimental conditions were such that the test gas was air, the mass flow rate was 10 g/s,

and the enthalpy was 18.5 MJ/kg. First of all, assuming a heating coefficient of 0.3, thermochemical equilibrium properties after arc heating were computed in the same manner as for the KU facility mentioned earlier. The factor of 0.3 accounts for the fact that the NAL facility has a plenum chamber downstream of the arc heater, so that the total enthalpy loss is expected to be more than that of the KU facility, which has no plenum chamber. Imposing these properties as upstream boundary conditions of the nozzle, nozzle computation was conducted. Computed nozzle entrance conditions of the NAL facility were $p = 16.9$ kPa, $T = 2900$ K, and $u = 1.12 \times 10^3$ m/s. The equilibrium temperature, 2900 K, immediately after arc heating is lower than 11,700 K at the KU facility. Although the arc power of the NAL facility is larger than that of the KU facility, the mass flow rate of the test gas in the NAL facility is higher than that of the KU facility by a factor of 20.8, which implies that the enthalpy per unit mass of the NAL facility is less than that of the KU arcjet facility. This could be why the temperature established after the arc heating at the KU facility is higher than that at the NAL facility. Calculated species mass fractions are shown in Table 4, from which it is seen that the dominant species are N_2, O, O_2, and NO. Two species, N_2^+ and NO^+, are no longer dominant species, although they were dominant species in the KU facility.

On-axis temperatures in the nozzle are depicted in Fig. 8. Unlike the result shown in Fig. 5, rapid relaxation of the O_2 and NO vibration cannot be seen. This is due to relatively low temperature at the nozzle entrance.

Computed on-axis flow properties at the nozzle exit are $p = 92.1$ Pa and $M = 4.7$, and on-axis temperatures there are shown in Table 5. Computed NO rotational temperature is 730 K, whereas measured temperature varies from 400 ± 50 K for $\delta(0,3)$ to 825 ± 25 K for $\gamma(0,1)$ as shown in Table 3. Except for $\delta(0,3)$, the computed results differ from the measured ones with an error of 10–13%.

Table 3 NO rotational temperature (K) measured at NAL arcjet facility

$\delta(0,1)$	$\delta(0,2)$	$\delta(0,3)$	$\gamma(0,0)$	$\gamma(0,1)$
660 ± 40	670 ± 30	400 ± 50	670 ± 40	825 ± 25

Table 4 Computed species mass fractions at nozzle throat of NAL arcjet facility

N_2	O	O_2	NO	NO^+
7.46×10^{-1}	1.11×10^{-1}	9.85×10^{-2}	4.45×10^{-2}	8.27×10^{-4}
N_2^+	N	N^+	O_2^+	O^+
1.87×10^{-4}	7.32×10^{-5}	9.02×10^{-10}	9.02×10^{-14}	2.44×10^{-16}

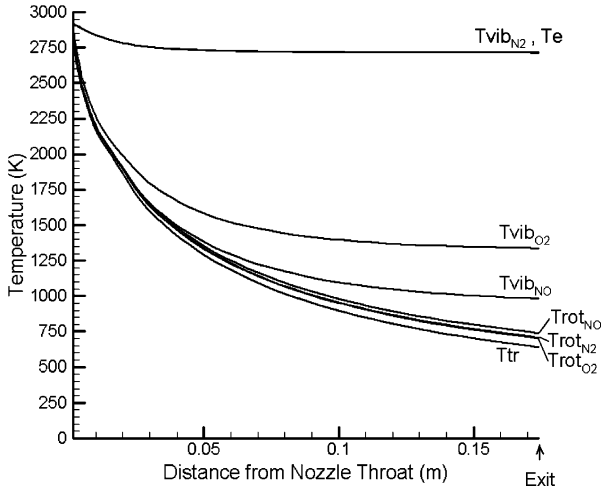

Fig. 8 On-axis temperature profiles in nozzle of NAL arcjet facility.

Table 5 Computed temperatures (K) at nozzle exit of NAL arcjet facility

T_{tr}	T_{rot,N_2}	T_{rot,O_2}	$T_{rot,NO}$
630	690	690	730
T_{vib,N_2}	T_{vib,O_2}	$T_{vib,NO}$	T_{tr}
2,700	1,300	980	2,700

As mentioned earlier, the comparison between measured NO rotational temperature and corresponding computed value in the KU facility shows an error of about 30%. At present, we have no complete explanation for this discrepancy, but some factors are to be focused on. Although the arc power in the NAL facility is higher than that in the KU facility, the mass flow rate in the NAL facility is also much higher and the on-axis temperature in NAL is rather lower than that in KU. Moreover, the NAL facility has a segment-type arc heater, which is much longer in the streamwise direction than the arc heater in the KU facility. This also means that the NAL facility provides a longer time period of arc heating. These facts may indicate that the flow condition in the NAL facility could achieve the thermochemical equilibrium state more sufficiently, which is assumed in the present study in calculating properties at the throat.

Conclusions

The processes of high-temperature air expansion in thermal nonequilibrium within a nozzle were numerically studied using a multiple vibrational and rotational temperature model. The result indicated that rotational temperatures of molecular species are close to being in equilibrium with each other, whereas the rotational temperatures are completely in nonequilibrium with translational temperature. This evidence implies that rotational temperature should be treated separately from translational temperature. In addition, emission spectra of NO at the wavelengths 220–265 nm were measured at the nozzle exit in the arcjet facility with air as the test gas. NO rotational temperature was determined by a curve-fitting procedure on NO $\gamma(0,1)$ band spectra. The experimental NO rotational temperature of 2500 K was compared with the computational one of 1800 K, showing 28% underestimation. Furthermore, the present computational analysis was applied to the arcjet facility of NAL, which was operated at a higher arc power than that in the present arcjet facility. The NO rotational temperature computed for the nozzle of the NAL arcjet facility was 730 K. This was compared with the experimental NO rotational temperature, which was determined by a curve-fitting procedure (different from SPRADIAN). Except for $\delta(0,3)$, the computed result differs from the measured ones with an error of only 10–13%. Based on comparisons between numerical and experimental results for these two different arc-jet facilities, it may be generally mentioned that the present analysis can approximately predict NO rotational temperature of arc-heated high-temperature air at the nozzle exit within an error of about 30%.

Acknowledgments

This research was partially supported by Grant-in-Aids for Scientific Research 15360450 and 15106013, sponsored by the Ministry of Education, Culture, Sports, Science and Technology, Japan.

References

[1]Babikian, D. S., Gopaul, N. K. J. M., and Park, C., "Measurement and Analysis of Nitric Oxide Radiation in an Arcjet Flow," *Journal of Thermophysics and Heat Transfer*, Vol. 8, No. 4, 1994, pp. 737–743.

[2]Babu, V., and Subramaniam, V. V., "Numerical Solutions to Nozzle Flows with Vibrational Nonequilibrium," *Journal of Thermophysics and Heat Transfer*, Vol. 9, No. 2, 1995, pp. 227–232.

[3]Park, C., and Lee, S.-H., "Validation of Multitemperature Nozzle Flow Code," *Journal of Thermophysics and Heat Transfer*, Vol. 9, No. 1, 1995, pp. 9–16.

[4]Nishida, M., and Matsumoto, M., "Thermochemical Nonequilibrium in Rapidly Expanding Flows of High-Temperature Air," *Zeitschrift für Naturforschung, Teil A: Physik, Physikalische Chemie, Kosmophysik*, Vol. 52, 1996, pp. 358–368.

[5]Bourdon, A., Leroux, A., Domingo, P., and Vervisch, P., "Experiment–Modeling Comparison in a Nonequilibrium Supersonic Air Nozzle Flow," *Journal of Thermophysics and Heat Transfer*, Vol. 13, No. 1, 1999, pp. 68–75.

[6]Winter, M. W., and Auweter-Kurtz, M., "Emission Spectroscopic Measurements of Temperatures and Boundary Layer Effects in Front of a Blunt Body in a Subsonic Air Plasma flow," AIAA Paper 99-3498, June 1999.

[7]Lago, V., Lebéhot, Dudeck, M., Pellerin, S., Renault, T., and Echegut, P., "Entry Conditions in Planetary Atmospheres: Emission Spectroscopy of Molecular Plasma Arcjets," *Journal of Thermophysics and Heat Transfer*, Vol. 15, No. 2, 2001, pp. 168–175.

[8]Yos, J. M., "Transport Properties of Nitrogen, Hydrogen, Oxygen and Air to 30,000 K," Technical Memorandum RAD TM-63-7, AVCO-RAD, Wilmington, MA, March 1963.

[9]Gupta, R. N., Yos, J. M., Thompson, R. A., and Lee, K.-P., "A Review of Reaction Rates and Thermodynamic and Transport Properties for an 11-Species Air Model for Chemical and Thermal Nonequilibrium Calculations to 30,000 K," NASA RP 1232, Aug. 1990.

[10]Lumpkin, "Development and Evaluation of Continuum Models for Translational–Rotational Nonequilibrium," Ph.D. dissertation, Stanford University, CA, 1990.

[11]Parker, J. G., "Rotational and Vibrational Relaxation in Diatomic Gases," *Physics of Fluids*, Vol. 2, No. 4, 1959, pp. 449–462.

[12]Millikan, R. C., and White, D. R., "Systematics of Vibrational Relaxation," *Journal of Chemical Physics*, Vol. 39, No. 12, 1963, pp. 3209–3213.

[13]Lee, J.-H., "Basic Governing Equations for the Flight Regimes of Aeroassisted Orbital Transfer Vehicles," *Thermal Design of Aeroassisted Orbital Transfer Vehicles*, edited by H. F. Nelson, Progress in Astronautics and Aeronautics, Vol. 96, AIAA, New York, 1985, pp. 3–53.

[14]Gnoffo, P. A., Gupta, R. N., and Shin, J. L., "Conservation Equations and Physical Models for Hypersonic Air Flows in Thermal and Chemical Nonequilibrium," NASA TP-2867, 1989.

[15]Candler, G. V., and MacCormack, R. W., "Computation of Weakly Ionized Hypersonic Flows in Thermochemical Nonequilibrium," *Journal of Thermophysics and Heat Transfer*, Vol. 5, No. 3, 1991, pp. 266–273.

[16]Lee, J.-H., "Electron-Impact Vibrational Relaxation in High-Temperature Nitrogen," *Journal of Thermophysics and Heat Transfer*, Vol. 7, No. 3, 1993, pp. 399–405.

[17]Hirakawa, M., Abe, K., Nishida, M., Takeishi, K., and Matsuura, M., "Application of a 20 kW Arc-Heated Wind Tunnel to Evaluation Tests of Wall Catalysis," *Transactions of Japan Society for Aeronautical and Space Sciences*, Vol. 45, Feb. 2003, pp. 217–223.

[18]Kim, K., Rho, O., and Park, C., "Navier–Stokes Computation of Flows in Arc Heaters," *Journal of Thermophysics and Heat Transfer*, Vol. 14, No. 2, 2000, pp. 250–258.

[19]Park, C., Raiche, II, G. A., Driver, D. M., Olejniczak, J., Terrazas-Slinas, I., Hightower, T. M., and Sakai, T., "Comparison of Enthalpy Determination Methods for an Arc-Jet Facility," AIAA Paper 2004-0487, 2004.

[20]Yee, H. C., "A Class of High Resolution Explicit and Implicit Shock Capturing Method," NASA TM-101088, 1989.

[21]Park, C., "Rotational Relaxation of N_2 Behind a Strong Shock Wave," AIAA Paper 2002-3218, June 2002.

[22]Fujita, K., and Abe, T., "SPRADIAN, Structured Package for Radiation Analysis: Theory and Application," ISAS Report 669, Institute of Space and Aeronautical Science, Sagamihara, Japan, 1997.

[23]Watanabe, Y., Ishida, K., and Shirai, H., "Spectroscopic Analysis of NO Band Emissions from Arc-Heated Air Flows in a 750 kW Arc-Heated Wind Tunnel," National Aerospace Laboratory NAL TR-1417, Chofu, Japan, 2000.